EARTHQUAKE ENGINEERING AND STRUCTURAL DYNAMICS
Earthquake Engng. Struct. Dyn. **28**, 879–897 (1999)

AN EXPERIMENTAL STUDY OF TEMPERATURE EFFECT ON MODAL PARAMETERS OF THE ALAMOSA CANYON BRIDGE

HOON SOHN[1,*], MARK DZWONCZYK[2], ERIK G. STRASER[1], ANNE S. KIREMIDJIAN[1], KINCHO H. LAW[1] AND TERESA MENG[2]

[1] *Department of Civil and Environmental Engineering, Stanford University, Stanford, CA 94305, U.S.A.*
[2] *Department of Electrical Engineering, Stanford University, Stanford, CA 94305, U.S.A.*

SUMMARY

Damage detection techniques have been proposed to exploit changes in modal parameters and to identify the extent and location of damage in large structures. Most of such techniques, however, generally neglect the environmental effects on modal parameters. Such environmental effects include changes in loads, boundary conditions, temperature, and humidity. In fact, the changes due to environmental effects can often mask more subtle structural changes caused by damage. This paper examines a linear adaptive model to discriminate the changes of modal parameters due to temperature changes from those caused by structural damage or other environmental effects. Data from the Alamosa Canyon Bridge in the state of New Mexico were used to demonstrate the effectiveness of the adaptive filter for this problem. Results indicate that a linear four-input (two time and two spatial dimensions) filter to temperature can reproduce the natural variability of the frequencies with respect to time of day. Using this simple model, we attempt to establish a confidence interval of the frequencies for a new temperature profile in order to discriminate the natural variation due to temperature. Copyright © 1999 John Wiley & Sons, Ltd.

KEY WORDS: adaptive filter; modal parameters; temperature effect; Alamosa Canyon Bridge; damage detection

1. INTRODUCTION

Many techniques have been proposed to identify the extent and location of damage in large structures using changes in the structures' model parameters. These methods typically determine the baseline parameters through acquisition of forced or ambient vibration test data. Damage detection is then based on the premise that damage in the structure will cause changes in the measured vibration data. Existing methods, however, neglect the important effects of environmental changes on the underlying structure. Changes in load, boundary conditions, temperature and humidity can have a significant effect on the underlying natural frequencies of large civil structures. In fact, the changes in the modal parameters due to environmental factors can be much larger than those

* Correspondence to: Hoon Sohn, The John A. Blume Earthquake Engineering Center, Department of Civil and Environmental Engineering, Stanford University, Stanford, CA 94305-4020, U.S.A. E-mail: sohnhoon@leland.stanford.edu

Contract/grant sponsor: National Science Foundation; Contract/grant number: CMS-95261-2
Contract/grant sponsor: National Aeronautics and Space Administration; Contract/grant number: NAG2-1065

CCC 0098–8847/99/080879–19$17·50

Received 21 April 1998
Revised 17 December 1998

caused by structural damage. During damp weather, for example, concrete bridges in the United Kingdom are reported to absorb considerable amount of moisture, which thus increases their masses and alters their natural frequencies.[1] Before damage detection systems can be reliably employed to monitor real structures, the variability of the modal parameters must be quantified.

This paper mainly studies the thermal effects on the non-stationary responses of bridges due to temperature changes. Very few researchers have addressed such a problem. Churchward and Sokal[2] attempted to predict the temperature distribution within bridge sections and to determine longitudinal expansion and vertical deflection based on a three-year monitoring of a post-stressed concrete section of a bridge. The measured environmental parameters include ambient air temperature, solar radiation, hours of sunshine and the temperature on the top surface of the section. It is found that the temperature profile can be reasonably represented using two design variables, namely maximum differential temperature and base temperature. Wood[1] reported that the changes of bridge responses were closely related to the structural temperature based on the vibration tests of five bridges in the United Kingdom. Analyses based on the data compiled suggested that the variability of the asphalt elastic moduli due to temperature effects was a major contributor to the changes in the structural stiffness.

Askegaard and Mossing[3] tested a three-span RC footbridge to investigate if modal parameters can provide a long-term indication of structural deterioration or crack formation. Seasonal changes of modal parameters were also monitored for a three-year period, and about 10 per cent change in frequency was repeatedly observed for each year. The authors concluded that the change was partially attributed to the variation of ambient temperature. Moorty[4] attempted to relate the responses of a bridge to thermal environmental conditions. An analytical model was developed to obtain the temperature-induced movements and the associated stresses in the bridge. A field test was conducted on the Sutton Creek Bridge in Montana, U.S.A. The movements obtained from both the analytical model and the measured values showed significant expansion of the bridge deck as temperature increased. A comprehensive research program on the Confederation Bridge in Eastern Canada has started in the spring of 1997 and will continue over many years to evaluate the effect of temperature on the short-term and long-term behaviour of the bridge.[5] Data on temperature and strain in the various components of the bridge, movement at expansion joints and deformation of the piers have been collected hourly. The extensive data collected will be used to develop computer models for predicting temperature effects in concrete bridges.

This paper presents an adaptive filter that accommodates the changes in temperature to the damage detection system of a large-scale bridge. This system determines modal frequencies using conventional modal analyses, but is able to adapt its prediction of the underlying natural frequencies of the structure based upon a time–temperature profile. This allows the system to discriminate the changes of modal parameters due to temperature changes from those caused by other environmental factors or structural damage. For example, when the measured frequencies move outside the predicted confidence intervals, the system can provide a reliable indication that structural changes are likely caused by factors other than thermal effect. Actual data collected from the Alamosa Canyon Bridge in New Mexico are used to train and test the system.

The paper is organized as follows. The next section describes the experimental setup at the Alamosa Canyon Bridge. Section 3 presents the training of the adaptive filter and a selection procedure of temperature input variables. Section 4 presents the construction of confidence intervals for prediction, and the examination of prediction performance using real test data. The paper concludes with a discussion of future research in Section 5.

Figure 1. A side view of the Alamosa Canyon Bridge

2. DESCRIPTION OF THE ALAMOSA CANYON BRIDGE TEST

The Alamosa Canyon Bridge is located near the town of Truth or Consequences in southern New Mexico and is approximately aligned in the north and south direction. This bridge has seven independent spans and each span consists of a concreted deck supported by six W30 × 116 steel girders. The top flanges of the girders are embedded in the concrete slab. The roadway in a span is approximately 7·3 m (24 ft) wide and 15·2 m (50 ft) long. Along the length of each span, four sets of crossing braces are equally spaced. Figure 1 depicts a side view of the Alamosa Canyon Bridge. More detailed description of the bridge can be found in Reference 6.

A new bridge has been constructed adjacent to this *old* Alamosa Canyon Bridge and since that time the tested bridge has not been used for regular traffic. During the past three years, however, the bridge has been tested several times by the Engineering Analysis Group of the Los Alamos National Laboratory (LANL). An attempt to characterize the natural variability of modal parameters was conducted in 1996.[6] The inherent uncertainty in the measured modal parameters was also studied using experimental test data from the bridge.[7]

This current study uses the results of the vibration tests conducted on July 27–August 2, 1996 and July 21–25, 1997, referred to here as the *first* and *second* data sets, respectively. The test data were provided to the authors by the Engineering Analysis Group of the LANL. The first data set was used to train the adaptive filter while the second data set was used to test the predictor. For both tests, only one span was implemented with sensors and tested. A total of 31 accelerometers were placed on the concrete deck and on the girders below the bridge. Five accelerometers were spaced along the length of each girder. Since there were six girders, a total of 30 accelerometers were placed on the girders. The last accelerometer was placed near the driving point. The time histories of accelerations and an excitation force were recorded, and the Frequency Response Functions (FRFs) were computed from the time histories. The FRFs were calculated for the range 0–50 Hz with the resolution of 0·0625 Hz. Thirty averages were used for all FRFs. An impact hammer which weighted approximately 53·4 N (12 lbs) was used to excite the bridge. The data acquisition for each test took 30–45 min. The modal parameters were extracted using the Eigensystem Realization Algorithm (ERA).[8] Approximately nine meaningful modes were identified from the ERA within the range of 0–30 Hz.

At the same time, temperature measurements were made on nine different locations across the centre of the span. Figure 2 illustrates a cross-section view of the bridge and the distribution of the indoor/outdoor thermometers, as follows: The bottom west outdoor sensor (T_8) was attached to

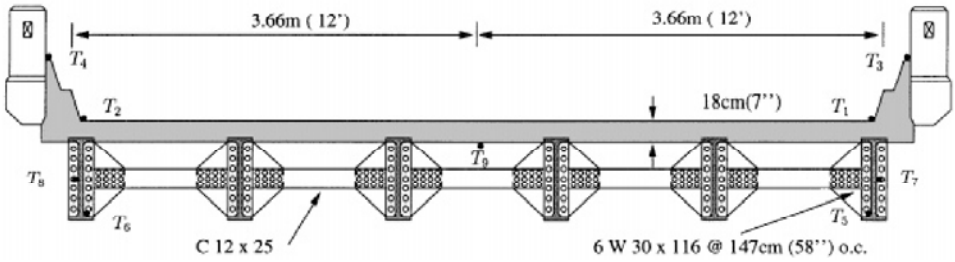

Figure 2. A cross-section view and thermometer locations of the Alamosa Canyon Bridge

the outside of the west-end exterior girder at the mid height of the web. The bottom west indoor sensor (T_6) was located on the inside bottom flange of the west-end exterior girder. The bottom centre sensor (T_9) was taped beneath the concrete deck at the centre of the span. The top west outdoor sensor (T_2) was located next to the concrete curb at the west-end of the deck. The top west indoor sensor (T_4) was placed on the top of the west-end guard rail. The four remaining sensors (T_1, T_3, T_5 and T_7) were placed on the east end of the span symmetrically to the west-end sensors. All sensors were protected from the direct contact with sunshine either by the bridge itself or by the shades made from duct tape and cups. However, the temperature measurements were not the most precise measurements that could have been made. Attempts were made to calibrate the thermometers prior to the tests, but the accuracy of the readings was not that which could be obtained with typical thermocouples.

The first vibration test was performed every 2 h over a 24-h time period to investigate the change of modal parameters with respect to time of day. The test started on July 31, 1996 at 09:15 and ended on August 1, 1996 at 9:22. The air was dry throughout the test. Farrar *et al.*[6] showed that the measured first mode frequency varied approximately 5 per cent during the 24-h test period, and the change in the measured fundamental frequency was found to correlate with the temperature difference across the deck. Similar variations and correlation with deck temperature difference were observed for the other modes of the bridge. Table I summarizes the measured frequencies and temperatures from the first vibration test. The temperature of a given time in Table I is an average of the thermometer readings before and after each vibration test. In addition to the temperature effect, traffic, winds, deterioration of the bridge and other environmental conditions could produce changes of the modal parameters. However, since the bridge was not used and the weather was calm during the test period, it is assumed that any changes of the modal parameters are mainly the result of the temperature changes.

The second test was conducted about one year after the first test. The second test started on July 22, 1997 at 04:00 and ended at midnight. Vibration tests were performed 11 times every 2 h. A note is in order about the weather conditions prior to the second vibration test; it had been raining hard from approximately 10:00 p.m. the previous night of the testing until 3:00 a.m. When the data acquisition was started at 4:00 a.m., rain was sufficient to produce ponds of water near the curbs and drainage paths were blocked by debris. The concrete deck was sufficiently cracked such that a fair amount of moisture might have been absorbed by the bridge. In the second testing, no temperature sensor was placed at the bottom centre. The other thermometers were placed almost in the same locations as those of the first testing. Table II summarizes the results from the second vibration test.

Table I. Summary of the first data set

Time	Freq. (Hz)		Temperature (°F)								
	1st	2nd	T_1	T_2	T_3	T_4	T_5	T_6	T_7	T_8	T_9
09:15	7·556	8·311	76·00	90·70	93·30	95·90	83·55	77·20	103·7	75·55	77·45
11:30	7·621	8·384	85·80	106·15	101·10	99·70	93·90	84·50	93·90	83·30	83·10
13:12	7·475	8·084	108·15	115·60	100·65	103·00	93·55	91·20	93·20	91·85	88·60
15:13	7·343	7·874	109·60	110·70	102·00	102·60	92·80	93·70	93·60	95·50	94·60
17:52	7·394	7·972	104·35	99·25	97·40	99·25	91·20	95·05	92·60	96·05	98·35
20:09	7·376	8·042	88·00	87·00	74·40	76·05	77·80	78·90	79·50	79·50	91·35
21:20	7·334	8·037	85·90	86·40	76·10	77·55	79·95	80·35	80·00	79·45	89·95
23:29	7·356	8·087	79·60	81·50	72·70	74·20	75·00	75·60	75·30	74·30	80·50
01:21	7·328	8·071	79·55	79·35	70·05	72·05	75·20	75·10	74·85	74·75	80·70
03:19	7·353	8·119	74·55	75·15	65·85	66·65	70·25	71·70	72·15	70·85	77·20
05:19	7·381	8·157	72·85	72·85	64·15	65·50	68·80	70·00	70·15	68·90	74·10
07:03	7·389	8·178	70·85	73·85	66·90	68·10	66·70	67·85	73·80	67·35	72·10
09:22	7·577	8·342	74·45	92·75	94·00	93·20	83·90	77·55	102·00	75·50	76·00

Table II. Summary of the second data set

Time	Freq. (Hz)		Temperature (°F)								
	1st	2nd	T_1	T_2	T_3	T_4	T_5	T_6	T_7	T_8	T_9
04:00	7·303	8·100	79·70	76·95	80·35	76·10	70·60	70·45	69·30	69·15	NA.
06:02	7·329	8·136	79·05	76·55	81·95	80·15	68·85	69·35	68·20	67·55	NA.
08:00	7·528	8·281	79·50	87·80	88·95	94·20	74·70	71·50	68·20	71·30	NA.
10:02	7·638	8·524	79·80	111·75	96·60	109·30	67·60	77·35	68·20	77·00	NA.
12:00	7·579	8·249	100·05	121·00	113·25	109·85	67·60	82·75	68·20	83·90	NA.
14:01	7·503	8·143	113·80	120·00	112·80	100·85	67·60	88·70	68·20	91·05	NA.
16:00	7·449	8·008	104·35	102·65	102·05	97·05	88·45	91·65	90·40	91·10	NA.
18:00	7·361	8·030	92·50	90·50	82·60	81·70	82·00	82·20	82·20	84·60	NA.
20:05	7·321	8·070	80·20	81·40	72·75	73·50	74·35	73·50	73·85	73·60	NA.
21:54	7·319	8·094	78·10	77·75	71·05	71·05	72·85	73·60	72·85	71·60	NA.
24:00	7·347	8·132	75·30	74·95	68·30	66·90	70·65	71·30	70·90	69·15	NA.

3. MODEL FORMULATION

First, prediction of the fundamental frequency was selected as a target for this study and the same procedure is repeated for the second mode frequency. It was presumed that the temperature changes of the bridge were mainly responsible for the variation of the frequencies. This assumption seems reasonable since the bridge was no longer in service and there was no significant change of weather conditions on the first test day. Observations of the bridge data coupled with some engineering judgment led to three additional assumptions that appear simplistic but are important factors in the design of the filter architecture: (1) changes in the modal parameters are *linearly* proportional to changes in temperature; (2) the mass of the bridge forced the change in modal parameters to lag behind the temperature, that is, the bridge takes some time to *warm up* and *cool off*; and (3) the geographical (north-south) orientation of the structure with respect to the sun suggests that the temperature of the west end of the bridge will have a time-lag behind the temperature of the east end.

Given these assumptions, a linear predictor is chosen as a system architecture. A linear filter simply creates a linear one-to-one mapping on input and output pairs. It affords explicit calculation of the filter coefficients using a simple matrix calculation and allows future modification of these coefficients using adaptive least-mean-squares-error minimization. The filter operates in two modes: *training* and *prediction*. Training is described in this section. Section 4 describes a validation regarding the applicability of the filter for prediction by testing its performance on the second data set.

3.1. Training the linear filter model

The architecture of the linear filter takes a subset of the temporal and spatial temperature profiles as inputs and delivers a single output that represents the estimated, or predicted, fundamental frequency. (Later, the same procedure is repeated for the second mode frequency.) In this sense, the filter is also a *multiple linear regression model*, but is more commonly termed a predictor or estimator. Determining the appropriate subset of the available temperature profiles is termed the *variable selection problem* and is discussed in Section 3.2. The method of *Least-Mean-Squares* (LMS) error minimization is used to estimate the coefficients of the predictor.[9]

The filter models the relationship between the selected bridge temperature inputs, $\mathbf{x} = [x_1\ x_2\ \ldots\ x_r]^{\mathrm{T}}$, a column vector of r inputs, and its measured fundamental frequency, y, at that temperature profile as a linear function:

$$y = w_0 + \mathbf{x}^{\mathrm{T}}\mathbf{w} + \varepsilon \tag{1}$$

where w_0 is bias or offset, $\mathbf{w}$ is a column vector of coefficients that weighs each temperature input, and ε is the *filter error*. Equation (1) can be rewritten to account for the offset term w_0 by redefining the input and weight vectors to have $p\ (= r + 1)$ dimensions:

$$y = \mathbf{x}^{\mathrm{T}}\mathbf{w} + \varepsilon \tag{2}$$

where $\mathbf{x} = [1\ x_1\ x_2\ \ldots\ x_r]^{\mathrm{T}}$ and $\mathbf{w} = [w_0\ w_1\ \ldots\ w_r]^{\mathrm{T}}$. Figure 3 depicts the filter to implement this model. In order to consider both the time and spatial variation of temperature, the temperature readings at the current time T_i and the previous time T_i' are used as input variables. That is, $\mathbf{x} = [\ 1\ T_1\ \ldots\ T_9\ T_1'\ \ldots\ T_9'\ ]^{\mathrm{T}}$ in Figure 3. The filter imposes a strictly linear mapping.

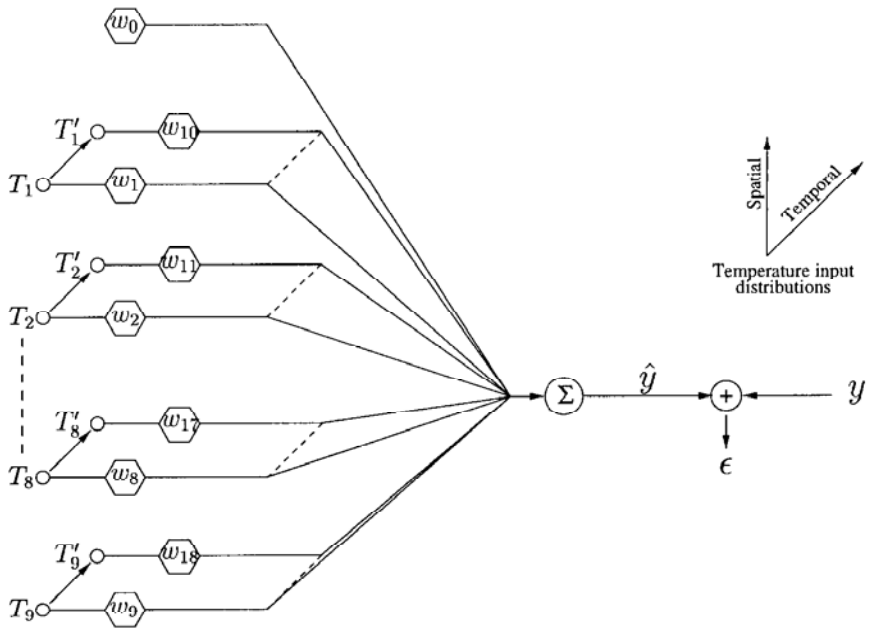

Figure 3. A linear adaptive filter

Suppose that n observations are available and let $\mathbf{x}(i)$ and $y(i)$ denote the ith input–output pairs. Equation (2) can be written in matrix notation:

$$\mathbf{y} = \mathbf{X}\mathbf{w} + \boldsymbol{\varepsilon} \tag{3}$$

where with n observations

$$\mathbf{y} = \begin{bmatrix} y(1) \\ y(2) \\ \vdots \\ y(n) \end{bmatrix}, \qquad \mathbf{X} = \begin{bmatrix} 1 & x_1(1) & x_2(1) & \dots & x_r(1) \\ 1 & x_1(2) & x_2(2) & \dots & x_r(2) \\ \vdots & \vdots & \vdots & & \vdots \\ 1 & x_1(n) & x_2(n) & \dots & x_r(n) \end{bmatrix}, \qquad \boldsymbol{\varepsilon} = \begin{bmatrix} \varepsilon(1) \\ \varepsilon(2) \\ \vdots \\ \varepsilon(n) \end{bmatrix}$$

The LMS error minimization is employed to estimate the filter coefficients. We wish to find the vector of the filter coefficients $\mathbf{w}$ that minimizes the expected value of the square of the filter error

$$\min_{\mathbf{w}} E[\varepsilon(i)^2] \tag{4}$$

where $E[\varepsilon(i)^2]$ is the mean of the filter errors created by n observations. $E[\varepsilon(i)^2]$ can be rewritten as follows. The index i is omitted for notational simplicity after the first line.

$$\begin{aligned} E[\varepsilon(i)^2] &= E[(y(i) - \mathbf{w}^{\mathrm{T}}\mathbf{x}(i))^2] \\ &= E[(y - \mathbf{w}^{\mathrm{T}}\mathbf{x})^2] \\ &= E[y^2 + \mathbf{w}^{\mathrm{T}}\mathbf{x}\mathbf{x}^{\mathrm{T}}\mathbf{w} - 2y\mathbf{x}^{\mathrm{T}}\mathbf{w}] \end{aligned}$$

$$= E[y^2] + \mathbf{w}^{\mathrm{T}} E[\mathbf{x}\mathbf{x}^{\mathrm{T}}]\mathbf{w} - 2E[y\mathbf{x}^{\mathrm{T}}]\mathbf{w}$$
$$= E[y^2] + \mathbf{w}^{\mathrm{T}}\mathbf{R}\mathbf{w} - 2\mathbf{p}^{\mathrm{T}}\mathbf{w} \tag{5}$$

where $\mathbf{R}$ ($=E[\mathbf{x}\mathbf{x}^{\mathrm{T}}]$) is the *autocorrelation* of the random input vector $\mathbf{x}$, and $\mathbf{p}$ ($=E[y\,\mathbf{x}^{\mathrm{T}}]$) is the *cross-correlation* between the desired output and the input vector. We note that $E[\varepsilon^2]$ is quadratic with $\mathbf{w}$ and thus can be solved for a single extrema (minima) with respect to $\mathbf{w}$. The *estimated* coefficients, $\hat{\mathbf{w}}$, are found by differentiating equation (6) with respect to $\mathbf{w}$ and setting the result equal to zero:

$$\nabla(E[\varepsilon^2])\frac{\partial E[\varepsilon^2]}{\partial \mathbf{w}} = 2(\mathbf{R}\hat{\mathbf{w}} - \mathbf{p}) = 0 \tag{6}$$

Solving for $\hat{\mathbf{w}}$,

$$\hat{\mathbf{w}} = \mathbf{R}^{-1}\mathbf{p} \tag{7}$$

Equation (7) is called the *Wiener–Hopf equation* and is used to determine the estimated coefficients, $\hat{\mathbf{w}}$, for a given set of input–output pairs.

One should note that the actual filter output error that results after applying the Wiener–Hopf equation is dependent upon the number of input–output mappings (n) that are used to determine $\hat{\mathbf{w}}$ and the dimension of $\hat{\mathbf{w}}$, p. If the filter is under-specified, that is, the number of input–output pairs is less than the dimension of $\hat{\mathbf{w}}$, then the Wiener–Hopf equation will produce an unlimited number of different $\hat{\mathbf{w}}$'s that result in zero error ($\boldsymbol{\varepsilon} = \mathbf{0}$). This means that there exists an infinite number of weights that will produce zero error for the given observation sets.

Since the training data set was fixed for this study, we decided to reduce the dimension p. In the derivation of equation (1), all input variables are assumed to be influential in predicting the output response. However, in most practical applications, the analyst must check the significance of each input and determine some optimal subset of inputs from a pool of *candidate* inputs. This variable selection is equivalent to pruning irrelevant or redundant inputs from the filter of Figure 3, and the procedure is addressed in the following subsection.

3.2. Input variable selection

We presume that the changes of the fundamental frequency are related to the spatial and temporal variations of temperatures across the bridge. In order to consider both the time and spatial variations of temperature, we decide to define the temperature readings at the current time T_i, and at the previous time T_i' as an initial pool of candidate input variables. Let k denote the size of this input pool. While the number of candidate input variables are 18 (nine temperature readings at the current time and the other nine from the one step previous time), the number of observations from the first vibration test is 13 ($n = 13$). Therefore, the selection of input variables should be conducted to reduce the size of the filter before any estimation of the filter coefficients. In general, a model with smaller number of input variables are more desirable because the variance of the prediction $\hat{y}$ increases as the number of inputs increases. Also, addition of extra inputs increases the costs of data collection and model maintenance.

First, the correlation of the nine sensor readings and the measured fundamental frequency is investigated. Table III presents the resulting correlation matrix. The correlation matrix shows that temperatures at the top east indoor (T_3) and at the top west indoor (T_4) are very closely related. (Figure 2 shows the locations of the thermometers.) The temperature at the bottom west indoor

Table III. Correlation of the measured fundamental frequency and the thermometer readings

	y	T_1	T_2	T_3	T_4	T_5	T_6	T_7	T_8	T_9
y	1·000									
T_1	−0·097	1·000								
T_2	0·435	0·835	1·000					Sym.		
T_3	0·608	0·684	0·941	1·000						
T_4	0·580	0·707	0·943	0·997	1·000					
T_5	0·485	0·787	0·969	0·966	0·966	1·000				
T_6	0·130	0·949	0·901	0·839	0·853	0·916	1·000			
T_7	0·741	0·396	0·750	0·910	0·909	0·807	0·605	1·000		
T_8	0·065	0·968	0·883	0·804	0·820	0·886	0·996	0·556	1·000	
T_9	−0·232	0·886	0·641	0·518	0·540	0·668	0·870	0·283	0·889	1·000

(T_6) is also strongly correlated to the temperature at the bottom west outdoor (T_8). T_4 is deleted from the filter model because T_3 has a larger correlation with the observation output y than T_4. For the same reason, T_6 is kept in the model and T_8 is excluded. Since the second data set did not measure the temperature at the bottom centre, the variable selection did not include T_9. Now, the number of candidate input variables becomes 12 ($k = 12$).

Next, an exhaustive search of all possible subsets of the remaining input variables is conducted using the Statistical Analysis System (SAS) program and the exhaustive search took on a SUN ULTRA-2 workstation less than a minute. If the intercept weight w_o is always included, a total of 2^k models should be examined. In this example, there are 2^{12} ($=4096$) possible models. This study employs *adjusted R^2 statistic* for comparing different models. To explain adjusted R^2 statistic, let R_p^2 denote the coefficient of multiple determination for a model with reduced size $p (\leqslant k+1)$. Computationally,

$$R_p^2 = \frac{\mathrm{SS_R}(p)}{S_{yy}} = 1 - \frac{\mathrm{SS_E}(p)}{S_{yy}} \tag{8}$$

and

$$S_{yy} = \sum_{i=1}^{n} [y(i) - \bar{y}]^2, \quad \mathrm{SS_R}(p) = \sum_{i=1}^{n} [\hat{y}(i) - \bar{y}]^2, \quad \mathrm{SS_E}(p) = \sum_{i=1}^{n} [y(i) - \hat{y}(i)]^2 \tag{9}$$

where S_{yy}, $\mathrm{SS_R}(p)$ and $\mathrm{SS_E}(p)$ denote the *total sum of squares*, the *regression sum of squares*, and the *residual sum of squares* of a model with p weightings, respectively. Furthermore, $\bar{y}$ denotes the mean of the output observation ($\bar{y} = \sum_{i=1}^{n} y(i)/n$) and n is the number of observations. R_p^2 increases as additional input variables are introduced to the model and reaches the maximum when $p = k + 1$.

The analyst might use this criterion by adding input variables to the model up to the point where an additional variable is not useful in that it provides only a small increase in R_p^2. However, since R_p^2 increases as p increases, using R_p^2 to determine the optimal models is not straightforward. To avoid this difficulty, this study prefers to use an adjusted R^2 statistic defined as:[10]

$$\bar{R}_p^2 = 1 - \left(\frac{n-1}{n-p}\right)(1 - R_p^2) \tag{10}$$

Note that $\bar{R}_p^2$ statistic does not necessarily increase as p increases. Consequently, one can consider the model that has the maximum $\bar{R}_p^2$ value an optimum model.

Table IV shows the five best models that maximize $\bar{R}_p^2$ for each given number of inputs, $3 \leqslant r \leqslant 9$. The first column of Table IV shows the identification numbers of the examined models. The best models for each given r ($3 \leqslant r \leqslant 9$) are retained for further comparison (models 1, 6, 11, 16, 21, 26 and 31). Note that three models (models 21, 22, and 23) with five input variables and model 26 with four inputs have larger $\bar{R}_p^2$ values than the models (models 11 and 16) with the largest $\bar{R}_p^2$ values for $r = 7$ and $r = 6$. Therefore, models 22 and 23 are also retained for further investigation. The filter system appears to approach the optimal architecture in terms of $\bar{R}_p^2$ statistic, when the size of inputs is about four or five ($4 \leqslant r \leqslant 5$).

Furthermore, we want to estimate the prediction performance of the model before future observations become available. A possible procedure is to split the training data into two parts: the *estimation data* and the *prediction data*. The estimation data is used to build the model, and the prediction data is employed to estimate the prediction capability of the model. The basic process is summarized as follows:[11]

1. Select an observation $y(i)$ as prediction data.
2. Fit the model to the remaining $n-1$ estimation data and use the model to predict the withheld observation (denote $\tilde{y}(i)$ as the predicted value corresponding to $y(i)$).
3. Compute the *deleted residual* defined as $e(i) = y(i) - \tilde{y}(i)$.
4. Repeat this procedure for all observations.

The Prediction Error Sum of Squares (PRESS) statistic is then defined as the sum of the deleted residuals. That is, $\text{PRESS} = \sum_{i=1}^{n} [y(i) - \tilde{y}(i)]^2$. Finally, an approximate R^2 for prediction is computed as:

$$R_{\text{pred}}^2 = 1 - \frac{\text{PRESS}}{S_{yy}} \tag{11}$$

This R_{pred}^2 is used as a complementary criterion and shown in the fourth column of Table IV.

For the remaining models (models 1, 6, 11, 16, 21, 22, 23, 26 and 31), two hypothesis tests (the F- and t-statistic tests) are conducted to measure model adequacy. These tests assume that the errors, $\varepsilon(i)$, in equation (3) are normally and independently distributed with zero mean and variance σ_ε^2. A detailed description for the F- and t-statistic tests can be found in Reference 10.

First, the F-statistic test determines if there is a linear relationship between the output and any of the input variables. The appropriate hypotheses are

$$\begin{aligned} &\text{H}_0\text{: } w_i = 0 \quad \text{for all } i \\ &\text{H}_1\text{: } w_i \neq 0 \quad \text{for at least one } i \end{aligned} \tag{12}$$

The hypothesis H_0 is rejected if $F_0 > F_{\alpha,r,n-r-1}$. Here, F_0 is a ratio of SS_R/r to $\text{SS}_\text{E}/(n-r-1)$, and $F_{\alpha,r,n-r-1}$ can be found from a statistical table of the F distribution. $\text{SS}_\text{R}/\sigma_\varepsilon^2$ and $\text{SS}_\text{E}/\sigma_\varepsilon^2$ have χ^2 distributions with r and $(n-r-1)$ degrees of freedom, respectively. Furthermore, $F_0 (= (n-r-1)\text{SS}_\text{R}/k\,\text{SS}_\text{E})$ have a F distribution with r and $n-r-1$ degrees of freedom for numerator and denominator, respectively. Rejection of H_0 implies that at least one of the inputs contributes significantly to the model. Table V presents the LMS estimation of the weighting coefficients and the F-statistic of the remaining models (models 1, 6, 11, 16, 21, 22, 23, 26 and 31). The last column of Table V shows that for all the selected models, the linear relationship between the

Table IV. The best five models for each given number of input variables

#	r	$\bar{R}^2$	R^2_{pred}	Selected input variables											
1*	9	0·99801	0·96958	T_1	T_2		T_5	T_6		T_1'		T_3'	T_5'	T_6'	T_7'
2		0·99718	0·98144	T_1	T_2	T_3		T_6		T_1'		T_3'	T_5'	T_6'	T_7'
3		0·99678	0·98716	T_1	T_2			T_6		T_1'	T_2'	T_3'	T_5'	T_6'	T_7'
4		0·99665	0·86686	T_1	T_2			T_6	T_7	T_1'		T_3'	T_5'	T_6'	T_7'
5		0·99424	0·72374	T_1	T_2			T_6	T_7	T_1'	T_2'	T_3'	T_5'		T_7'
6*	8	0·99747	0·99374	T_1	T_2			T_6		T_1'		T_3'	T_5'	T_6'	T_7'
7		0·99517	0·98352	T_1	T_2	T_3		T_6		T_1'		T_3'	T_5'		T_7'
8		0·99324	0·97479		T_2	T_3			T_7	T_1'	T_2'	T_3'	T_5'	T_6'	
9		0·99320	0·97169	T_1		T_3			T_7	T_1'	T_2'	T_3'	T_5'	T_6'	
10		0·99318	0·93469	T_1	T_2			T_6		T_1'	T_2'	T_3'	T_5'		T_7'
11*	7	0·99373	0·98514			T_3			T_7	T_1'	T_2'	T_3'	T_5'	T_6'	
12		0·99302	0·98485		T_2	T_3				T_1'	T_2'	T_3'	T_5'	T_6'	
13		0·99293	0·96718	T_1		T_3			T_7	T_1'	T_2'	T_3'	T_5'		
14		0·99277	0·96203	T_1	T_2	T_3			T_7		T_2'	T_3'	T_5'		
15		0·99275	0·97943		T_3		T_5	T_6	T_7		T_2'	T_3'	T_5'		
16*	6	0·99387	0·98804	T_1		T_3			T_7		T_2'	T_3'	T_5'		
17		0·99373	0·98639			T_3			T_7	T_1'	T_2'	T_3'	T_5'		
18		0·99369	0·98766			T_3		T_6	T_7		T_2'	T_3'	T_5'		
19		0·99360	0·98694			T_3			T_7		T_2'	T_3'	T_5'		T_7'
20		0·99358	0·98733			T_3				T_1'	T_2'	T_3'	T_5'	T_6'	
21*	5	0·99428	0·99112			T_3			T_7		T_2'	T_3'	T_5'		
22*		0·99414	0·99062	T_1		T_3			T_7		T_2'	T_3'			
23*		0·99386	0·99054		T_2	T_3			T_7		T_2'	T_3'			
24		0·99361	0·98613			T_3		T_6	T_7		T_2'	T_3'			
25		0·99351	0·98878			T_3			T_7		T_2'	T_3'			T_7'
26*	4	0·99410	0·99165			T_3			T_7		T_2'	T_3'			
27		0·98934	0·98275			T_3				T_1'	T_2'	T_3'			
28		0·98885	0·98131			T_3					T_2'	T_3'		T_6'	
29		0·98757	0·97702		T_2	T_3					T_2'	T_3'			
30		0·98735	0·97116			T_3	T_5				T_2'	T_3'			
31*	3	0·98809	0·97809			T_3					T_2'	T_3'			
32		0·94915	0·90774							T_1'		T_3'	T_5'		
33		0·94346	0·89520				T_5				T_2'	T_3'			
34		0·93581	0·89347			T_3					T_2'				T_7'
35		0·91828	0·87422			T_3					T_2'		T_5'		

* Theses models are retained for further comparison and investigation.

inputs and output is significant. However, the passing of the F-statistic test does not necessarily indicate that the model examined is an appropriate one for predicting the output. Further tests of model adequacy are required.

Next, the t-statistic test examines the significance of the individual filter coefficient to the model given the other inputs in the model. The hypotheses for testing the significance of any input, such

Table V. The estimated weights for the selected models

#	r	Estimated weightings						
		$\hat{w}_o$	$\hat{w}_{T_1}$ $(\times 10^{-2})$	$\hat{w}_{T_2}$ $(\times 10^{-3})$	$\hat{w}_{T_3}$ $(\times 10^{-3})$	$\hat{w}_{T_5}$ $(\times 10^{-3})$	$\hat{w}_{T_6}$ $(\times 10^{-2})$	$\hat{w}_{T_7}$ $(\times 10^{-3})$
1	9	7·457	−1·276	7·548		−4·179	1·419	
6	8	7·559	−1·102	5·346			0·964	
11	7	7·530			6·055			−1·162
16	6	7·572	−0·053		7·832			−2·358
21	5	7·580			7·478			−2·171
22	5	7·517	−0·070		8·105			−2·287
23	5	7·527		−0·633	8·462			−2·367
26	4	7·509			7·694			−1·992
31	3	7·429			5·957			
		$\hat{w}_{T'_1}$ $(\times 10^{-3})$	$\hat{w}_{T'_2}$ $(\times 10^{-2})$	$\hat{w}_{T'_3}$ $(\times 10^{-2})$	$\hat{w}_{T'_5}$ $(\times 10^{-2})$	$\hat{w}_{T'_6}$ $(\times 10^{-2})$	$\hat{w}_{T'_7}$ $(\times 10^{-3})$	$F_o(F_{\alpha,r,n-r-1})$
1	9	−9·258		1·303	−1·557	1·311	−5·822	670·487(>6·04)
6	8	−8·288		1·427	−1·475	1·029	−6·454	592·828(>4·88)
11	7	−4·049	−0·997	1·047	−0·785	0·628		272·680(>4·28)
16	6		−1·453	1·095	−0·186			325·259(>3·97)
21	5		−1·503	1·147	−0·232			418·202(>3·84)
22	5		−1·490	1·002				408·356(>3·84)
23	5		−1·573	1·050				389·600(>3·84)
26	4		−1·575	1·044				506·328(>3·86)
31	3		−1·480	1·005				332·842(>4·10)

as w_i, are

$$\begin{aligned} &H_0:\ w_i = 0 \\ &H_1:\ w_i \neq 0 \end{aligned} \tag{13}$$

If $|t_0| > t_{\alpha/2,n-r-1}$, the hypothesis H_0 is rejected implying that the examined input contributes significantly to the model. Here, $t_0 \left(= w_i / \sqrt{\hat{C}_i \, \sigma_\varepsilon^2}\right)$ has a t distribution, C_i is the ith diagonal element of $(X^T X)^{-1}$, and $\hat{\sigma}_\varepsilon^2$ is an unbiased estimate of the sum of squared errors of the system

$$\hat{\sigma}_\varepsilon^2 = \sum_{i=1}^{n} \frac{[y(i) - \hat{y}(i)]^2}{n - p} \tag{14}$$

The value of $t_{\alpha,r,n-r-1}$ is found from a statistical table of the t distribution. Note that this examines only the marginal contribution of one input given the other inputs are in the model. Table VI shows the results of the t-statistic test. Each filter coefficient that does not pass the t-statistic test is subscripted by an asterisk * in Table VI. Except for models 6, 26 and 31, the hypothesis H_0: $w_i = 0$ is not rejected. This indicates that the other models contain redundant inputs that can be deleted from the models.

Table VI. The t-statistic test of each weight for the selected models

ID#	r	t-statistic (t_o)						
		$\hat{w}_o$	$\hat{w}_{T_1}$	$\hat{w}_{T_2}$	$\hat{w}_{T_3}$	$\hat{w}_{T_5}$	$\hat{w}_{T_6}$	w_{T_7}
1	9	84·166	−7·548	4·629		−1·445*	4·292	
6†	8	125·900	−8·255	8·156			8·557	
11	7	72·692			4·313			−1·070*
16	6	103·642	−0·729*		9·824			−3·339
21	5	108·696			12·248			−3·416
22	5	247·207	−1·030*		11·420			−3·338
23	5	202·962		−0·832*	7·682			−3·033
26†	4	254·457			13·071			−3·188
31†	3	330·891			18·800			
		$\hat{w}_{T_1'}$	$\hat{w}_{T_2'}$	$\hat{w}_{T_3'}$	$\hat{w}_{T_5'}$	$\hat{w}_{T_6'}$	$\hat{w}_{T_7'}$	$t_{\alpha,r,n-r-1}$
1	9	−9·612		10·609	−10·160	5·281	−5·365	3·182
6†	8	10·639		14·386	−9·184	5·943	−5·763	2·776
11	7	−1·099	−2·247*	6·727	−1·465*	0·999*		2·571
16	6		−13·107	8·460	−0·830*			2·447
21	5		−17·902	11·023	−1·120*			2·365
22	5		−14·985	15·724				2·365
23	5		−27·998	20·699				2·365
24	5		−14·996	15·811				2·365
25	5		−18·894	8·911			0·519*	2·365
26†	4		−28·639	21·193				2·306
31†	3		−22·566	14·820				2·262

† Only these models pass the t-statistic test
* These coefficients do not pass the t-statistic test

Finally, model 26 with inputs T_3, T_7, T_2' and T_3' is selected as a *satisfactory* model for the prediction of the second data set since (1) the $\bar{R}_p^2$ value of model 26 is comparable to that of model 6 or better than model 31, (2) the R^2_{pred} value of model 26 is higher than the other models (except model 6), (3) this model passes both the F- and t-statistic tests, and (4) model 26 has only half as many inputs as model 6. From equation (7), the LMS estimator of $\hat{\mathbf{w}}$ is computed for model 26:

$$\hat{\mathbf{w}} = \begin{bmatrix} \hat{w}_o \\ \hat{w}_{T_3} \\ \hat{w}_{T_7} \\ \hat{w}_{T_2'} \\ \hat{w}_{T_3'} \end{bmatrix} = \begin{bmatrix} 7{\cdot}509 \\ 0{\cdot}007694 \\ -0{\cdot}001992 \\ -0{\cdot}01575 \\ 0{\cdot}01044 \end{bmatrix} \tag{15}$$

Usually, the selection of an optimal model is not a computationally trivial task. One should also check if the model is physically reasonable. The selection of model 26 and the estimated filter coefficients in equation (15) reveals that (1) the response change of the Alamosa Canyon Bridge lags the temperature of the bridge (the temperatures of two hours before the current time contribute more significantly to the change of the current frequency than the temperatures at the current time:

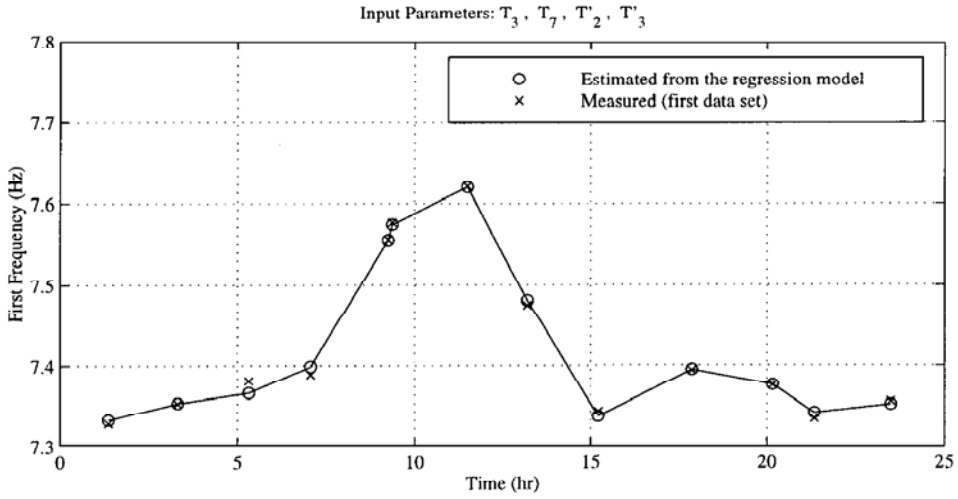

Figure 4. Reproduction of the first mode frequency using a linear filter

$\hat{w}_{T_2'}$ and $\hat{w}_{T_3'}$ are approximately ten times larger than $\hat{w}_{T_3}$ and $\hat{w}_{T_7}$), and (2) the temperature gradient between the top west outdoor and the top east indoor ($0{\cdot}01044T_3' - 0{\cdot}01575T_2'$) largely influences the variation of the fundamental frequency. This supports the observation in Reference 6 that the changes in modal frequencies are related to the temperature differentials across the deck.

Figure 4 shows how well the selected model 26 reproduces the first mode frequency from the first data set which is employed for the training of the filter. Note that only three temperature readings at the top west outdoor, top west indoor and bottom east outdoor out of the total of nine thermometers are necessary to reasonably estimate the change of the fundamental frequency.

4. PREDICTION USING A TRAINED MODEL

The adaptive filter established in the previous section was used to predict the fundamental natural frequency of the bridge. The predicted value is then used to discriminate the changes of the fundamental natural frequency caused by temperature effects from changes caused by other environmental effects or potential damage of the structure. For example, let $\mathbf{x}_0$ denote a vector of new temperature readings. A point prediction $\hat{y}_0$ of the fundamental natural frequency at the temperature profile becomes

$$\hat{y}_0 = \mathbf{x}_0^{\mathrm{T}} \hat{\mathbf{w}} \tag{16}$$

where $\hat{\mathbf{w}}$ is the weight vector determined from equation (15).

One can not expect a perfect match of the prediction and the measured modal parameters because of incompleteness of the model, insufficient training data sets, uncertainties in actual testing and measurements and so on. Of broader importance, however, one can compute a confidence interval around the point prediction $\hat{y}_0$ to account for the inherent uncertainties. The upper and lower

Table VII. Comparison of the measured fundamental frequency and the 95 per cent confidence intervals

Time	Confidence bounds		y	$\hat{y}$	Relative* error(%)	Extrapolation check h_0 ($h_{\max}$)
	Lower	Upper				
06:02	7·592	7·669	7·630	7·329	3·95	3·6004 (>0·7686)
08:00	7·660	7·755	7·707	7·528	2·32	5·9233 (>0·7686)
10:02	7·612	7·712	7·662	7·638	0·31	6·6219 (>0·7686)
12:00	7·435	7·550	7·493	7·579	1·15	9·0997 (>0·7686)
14:01	7·463	7·570	7·517	7·503	0·19	8·0356 (>0·7686)
16:00	7·379	7·424	7·401	7·449	0·64	0·5026 (<0·7686)
18:00	7·407	7·451	7·429	7·361	0·92	0·4734 (<0·7686)
20:05	7·338	7·378	7·358	7·321	0·51	0·1836 (<0·7686)
21:54	7·367	7·408	7·388	7·319	0·93	0·2384 (<0·7686)
24:00	7·389	7·431	7·410	7·347	0·85	0·3396 (<0·7686)

* Relative error $(\%) = 100 \times | y - \hat{y} | / \hat{y}$

bounds of a $100(1-\alpha)$ per cent confidence interval for the predicted output at the given input observation, namely $\hat{y}_0$ in this case, is computed as:[10]

$$\hat{y}_0 \pm t_{\alpha/2, n-p} \sqrt{\hat{\sigma}_\varepsilon^2 (1 + \mathbf{x}_0^{\mathrm{T}} (\mathbf{X}^{\mathrm{T}} \mathbf{X})^{-1} \mathbf{x}_0)} \tag{17}$$

Once the filter is trained, the newly measured frequency can be compared against the confidence interval. If the fundamental natural frequency falls outside the confidence interval, then one may suspect with the given confidence that some changes in the underlying structural characteristic are caused by damage or other effects. Table VII shows the predicted value of the fundamental frequency and a 95 per cent confidence interval computed at the different time of temperature profiles from the second data set. The first column of the table shows the starting time of each testing, and the second and third columns present the lower and upper bounds of the confidence interval, respectively. These bounds are computed from equation (17). The variables $\hat{y}$ and y in Table VII denote the predicted frequency from equation (16) and the measured frequency from the second testing, respectively.

In predicting new observations, one should be careful not to extrapolate beyond the input variable region containing the training data set. A model that fits well inside the region of the original data may perform poorly outside that region. In a multi-dimensional input space, it is difficult to decide if an input variable point lies inside or outside the region of the original data. The diagonal elements of the *hat* matrix $\mathbf{H} (= \mathbf{X}(\mathbf{X}^{\mathrm{T}}\mathbf{X})^{-1}\mathbf{X}^{\mathrm{T}})$ are employed to detect a hidden extrapolation point.[10] Let the largest diagonal value of the hat matrix $\mathbf{H}$ to be $h_{\max}$, and define the smallest convex surface containing all of the training data points as the input variable hull (IVH). The relative distance of any input variable vector $\mathbf{x}_0$ to the centroid of the IVH is reflected by

$$h_0 = \mathbf{x}_0^{\mathrm{T}} (\mathbf{X}^{\mathrm{T}} \mathbf{X})^{-1} \mathbf{x}_0 \tag{18}$$

If $h_0 > h_{\max}$, the point is outside the IVH and requires an extrapolation. The value of h_0 depends both on the Euclidean distance of the corresponding point from the centroid of the training data and on the density of points in the IVH. In the last column of Table VII, the h_0 value of each input is compared to $h_{\max}$. Only the last five points corresponding to time 16:00, 18:00, 20:05,

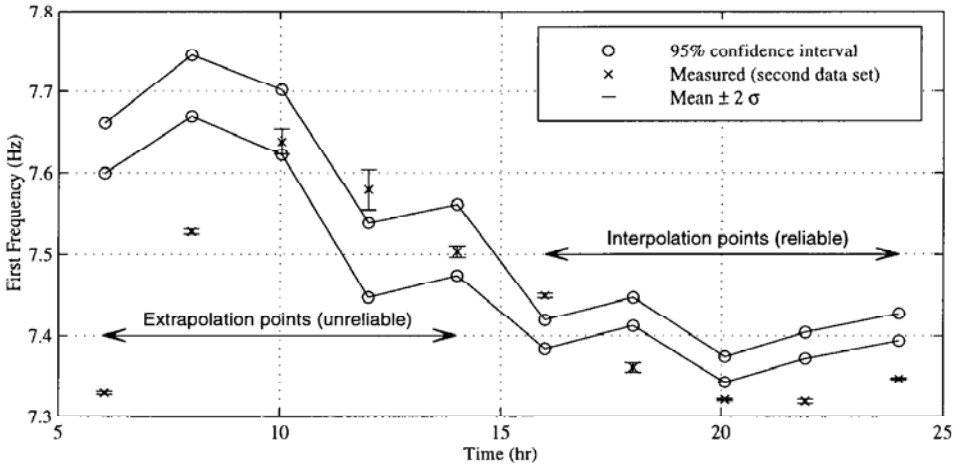

Figure 5. Prediction of the first mode frequency using a linear filter

21 : 54 and 24 : 00 are interpolation points. We presume that only these data points inside the IVH are reliable for the prediction.

The measured fundamental frequency from the second data set, and the upper and lower bounds of the 95 per cent confidence interval are plotted in Figure 5. Figure 5 reveals that the measured frequencies corresponding to the interpolation points are consistently lower than the associated lower bounds of the 95 per cent prediction interval (except the one at time 16 : 00). The linear filter was also trained using the second mode frequency from the first data set and tested for prediction of the second mode frequency from the second data set. Figures 6 and 7 show the reproduction of the training data set and the prediction result for the second mode frequency, respectively. Again we observe that the measured second frequency is lower than or close to the lower bound of the confidence interval.

This result implies that the stiffness of the structure is deteriorated and/or the mass of the structure is increased. Considering the facts that the Alamosa Canyon Bridge is a concrete bridge, it had visible cracks over the deck, there was a severe rain prior to the second test, and the drainage paths were filled with debris and dirt, it is very possible that these consistent decreases of the fundamental natural frequency were mainly caused by the increase of the bridge mass as the Alamosa Canyon Bridge absorbed significant amount of moisture and the bridge retained some of the rainfall on its surface. Assuming that the change of the bridge mass is solely responsible for the decrease of the fundamental frequencies within the interpolation points, the increase of mass is approximately estimated as 1·62 per cent. Considering the experimental study that several concrete bridges in the United Kingdom absorbed considerable amount of moisture during damp weather, and consequently increased the mass of the bridge approximately by 3–6 per cent,[12] the change of the mass estimated in this study falls within a reasonable range.

Note that statistical uncertainty bounds (mean $\pm 2\sigma$) are added around the measured frequencies in Figures 5 and 7 to show that the variation caused by thermal effect is larger than the inherent uncertainties in the measured frequencies (the measured frequencies in Figures 4–7 are the mean values computed by averaging 30 FRFs). The standard deviation (σ) of the frequencies is estimated using the procedure described in References 12 and 7.

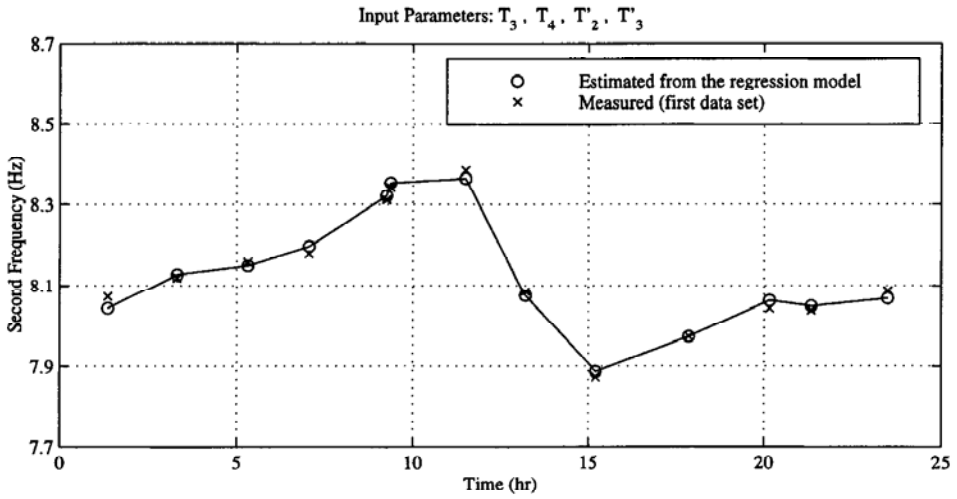

Figure 6. Reproduction of the second mode frequency using a linear filter

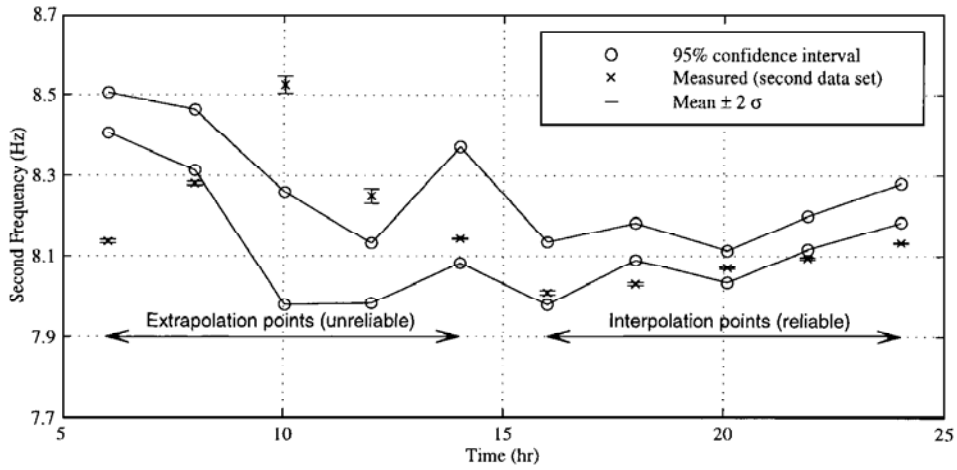

Figure 7. Prediction of the second mode frequency using a linear filter

5. SUMMARY AND DISCUSSIONS

This paper has presented an adaptive filter for predicting changes in modal parameters of a full-scale bridge due to environmental temperature. Data from the Alamosa Canyon Bridge in New Mexico were employed to demonstrate the applicability of the adaptive filter. The vibration tests were conducted during the summer of 1996 and 1997. The first data set from 1996 test was used to train the adaptive filter while the second data set from 1997 test was used to test the prediction performance.

Changes in the frequencies are found linearly correlated with temperature readings from different parts of the bridge. The filter uses spatial and temporal temperature distributions to determine changes in the first and second mode frequencies. The simplicity of the filter belies its importance: the filter is able to account for the non-stationarity in the frequencies caused by an environmental factor. A linear filter with two spatially separated temperature measurements and two temporally separated temperature measurements reproduces the variation of the frequencies of the first data set.

Based on the trained filter system, a prediction interval of the frequency for a new temperature profile is computed and the prediction performance is tested using the second data set. The system defines a confidence interval for future values of modal parameters in order to discriminate between variations caused by temperature changes and those indicative of structural change or other environmental effects. The comparison of the prediction intervals obtained from the first data set and the measured frequencies from the second test data reveals that the bridge experienced a statistically significant decrease in the first and second mode frequencies. Considering the severe rain prior to the testing and the drainage system severely blocked by debris, it is very possible that this consistent decrease of the frequencies was mainly caused by the increase of the bridge mass as the Alamosa Canyon Bridge absorbed significant amount of moisture, and the bridge retained much of the rainfall on its surface.

It should be kept in mind that the filter system presented was developed for a particular bridge under particular environmental conditions. Further and well controlled testings are required to fully validate this linear model. Although this study has been limited to a single external variable (temperature), the approach might be extendible to other environmental effects. To control for other environmental conditions and account for larger-scale seasonal variations, tests should be conducted during different times of the year as well as different times of a day, and measurements for other environmental factors should be obtained. Furthermore, a continuous data collection system would allow the filter coefficients to be more reliably updated, and to decrease the size of the confidence intervals. Last but not least, as shown in the test data, reliable damage detection must account for the significant non-stationary environmental processes. Continuous research is needed to develop reliable approach to deal with the sources of variability from field vibration tests.

ACKNOWLEDGEMENTS

The authors wish to express their sincere thanks to Dr Charles R. Farrar and Dr Scott W. Doebling of the Los Alamos National Laboratory for providing the experimental data of the Alamosa Canyon Bridge. This research was sponsored by the National Science Foundation under Grant No. CMS-95261-2 and the National Aeronautics and Space Administration under Grant No. NAG2-1065.

REFERENCES

1. M. G. Wood, '*Damage analysis of bridge structures using vibrational techniques*', *Ph.D. thesis*, Department of Mechanical and Electrical Engineering, University of Aston, Birmingham, UK, 1992.
2. A. Churchward and Y. J. Sokal, 'Prediction of temperatures in concrete bridges', *J. Struct. Div. ASCE* **107**, 2163–2176 (1981).
3. V. Askegaard and P. Mossing, 'Long term observation of RC-bridge using changes in natural frequencies', *Nordic Concrete Res.* **7**, 20–27 (1988).
4. S. Moorty and C. W. Roeder, 'Temperature-dependent bridge movements', *J. Struct. Engng.* **118**, 1090–1105 (1992).
5. W. H. Dilger and S. A. Loptson, 'Temperature monitoring of the Confederation Bridge', in *The Annual Conf. of the Canadian Society for Civil Engineering*, Quebec, Canada, 1997, pp. 151–160.

6. C. R. Farrar, S. W. Doebling, P. J. Cornwell and E. G. Straser,'Variability of modal parameters measured on the Alamosa Canyon Bridge', in *Proc. 15th Int. Modal Analysis Conf.* Orlando, FL, 1997, pp. 257–263.
7. S. W. Doebling, C. R. Farrar and R. S. Goodman, 'Effects of measurement statistics on the detection of damage in the Alamosa Canyon Bridge', in *Proc. 15th Int. Modal Analysis Conf.*, Orlando, FL, 1997, pp. 918–929.
8. J. N. Juang, 'An Eigensystem Realization Algorithm for modal parameter identification and model reduction', *J. Guidance Control Dyn.* **8**, 620–627 (1985).
9. B. Widrow and S. D. Stearns, *Adaptive Signal Processing*, Prentice-Hall, Englewood Cliffs, NJ, 1985.
10. D. C. Montgomery and E. A. Peck, *Introduction to Linear Regression Analysis*, Wiley, New York, 1991.
11. D. M. Allen, 'The relationship between variable selection and data augmentation and a method for prediction', *Technometrics* **16**, 125–127 (1974).
12. J. S. Bendat and A. G. Piersol, *Engineering Applications of Correlation and Spectral Analysis*, Wiley, New York, 1980.

